Dissipative Light Bullets in Kerr Cavities: Multistability, Clustering, and Rogue Waves

S. S. Gopalakrishnan,[1,2,*] K. Panajotov,[3,4] M. Taki,[2] and M. Tlidi[1]
[1]Faculté des Sciences, Université libre de Bruxelles (U.L.B), CP. 231, 1050 Brussels, Belgium
[2]Université Lille, CNRS, UMR 8523—PhLAM—Physique des Lasers, Atomes et Molécules, F-59000 Lille, France
[3]Department of Applied Physics and Photonics (IR-TONA), Vrije Universiteit Brussels, Pleinlaan 2, 1050 Brussels, Belgium
[4]Institute of Solid State Physics, 72 Tzarigradsko Chaussee Boulevard, 1784 Sofia, Bulgaria

(Received 17 November 2020; revised 3 February 2021; accepted 19 March 2021; published 16 April 2021)

We report the existence of stable dissipative light bullets in Kerr cavities. These three-dimensional (3D) localized structures consist of either an isolated light bullet (LB), bound together, or could occur in clusters forming well-defined 3D patterns. They can be seen as stationary states in the reference frame moving with the group velocity of light within the cavity. The number of LBs and their distribution in 3D settings are determined by the initial conditions, while their maximum peak power remains constant for a fixed value of the system parameters. Their bifurcation diagram allows us to explain this phenomenon as a manifestation of homoclinic snaking for dissipative light bullets. However, when the strength of the injected beam is increased, LBs lose their stability and the cavity field exhibits giant, short-living 3D pulses. The statistical characterization of pulse amplitude reveals a long tail probability distribution, indicating the occurrence of extreme events, often called rogue waves.

DOI: 10.1103/PhysRevLett.126.153902

Localized structures (LSs) and localized patterns are dissipative structures found far from equilibrium that have been observed in many areas of natural science, such as chemistry, physics, biology, and plant ecology [1]. Nonlinear optics and laser physics provide classic examples of LSs that can be experimentally investigated in a reliable way [2]. In one-dimensional (1D) dispersive driven cavities, they have been theoretically predicted [3] and experimentally demonstrated [4,5]. Their link to frequency combs was established in [6] and has reinforced the interest in this field of research. Their spectral contents correspond to optical frequency combs, which have applications in metrology and spectroscopy [7].

In broad area cavities where two-dimensional (2D) diffraction cannot be ignored, LSs have been experimentally observed as well [8]. They are addressable structures with a possibility for applications in all-optical control of light, optical storage, and information processing [8]. Apart from these applications in 1D and 2D settings, LSs are of general interest in other fields of active research such as hydrodynamics, Bose–Einstein condensates, biology, and plant ecology [8].

From a theoretical point of view, the challenging aspect lies in the collapse of LSs for the case of the nonlinear Schrödinger equation when the dimensionality of the system is at least 2 [9]. To prevent wave collapse in three-dimensional settings, it is necessary to introduce additional physical effects, such as optical cavity [10], semiconductor active media [11], saturable absorbers [12], parametric oscillators [10], or twisted waveguide arrays [13] (see recent reviews [2,8,14]).

The purpose of this Letter is to predict the occurrence of stable stationary light bullets (LBs) in the dispersive and diffractive driven Kerr resonators. These three-dimensional (3D) dissipative structures can be either isolated or bound together or form self-organized clusters. Some of these structures have been reported close to the nascent bistability regime [15]. We characterize these 3D solutions by constructing their bifurcation diagram and determine their range of stability. This diagram exhibits multistability, which clearly indicates that clustering phenomenon belongs to a homoclinic snaking type of bifurcation. When increasing the injected field power, we observe transition via period doubling to a complex dynamical regime. In this regime, statistical analyses show that the amplitude probability distribution possesses a long tail with pulse intensity height well beyond 2 times the significant wave height (SWH) [16]. The SWH is defined as the mean height of the highest third of waves. From these two characteristics, we can infer that this complex behavior belongs to the class of rogue waves. In optics, rogue waves have been first observed in one-dimensional settings by Solli *et al.* [17]. Finally, we provide experimentally relevant parameters based on chalcogenide glass, which possesses a very strong Kerr effect and responds instantaneously to electrical excitation.

We consider a Fabry–Perot cavity filled with Kerr medium and coherently driven by an external injected field E_i. The transmitted part of this field will interact with the nonlinear media and suffer from nonlinearity, diffraction, chromatic dispersion, and losses. The schematic setup of an optical cavity filled with a Kerr medium is shown in Fig. 1.

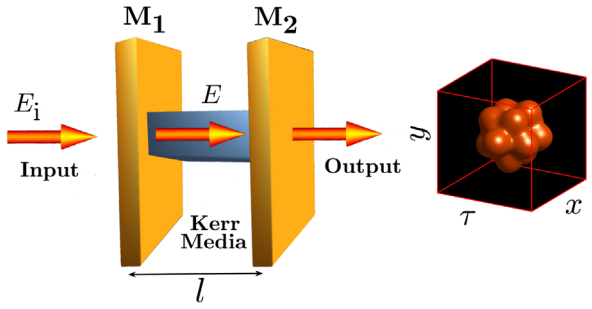

FIG. 1. Schematic setup of an optical cavity filled with a Kerr medium. An injected field E_i is launched inside the cavity by means of the mirror M_1. The input M_1 and the output M_2 mirrors are separated by a distance l and are identical. The resulting field circulating within the cavity after several round-trips is denoted by E. A possible output consisting of a cluster involving 14 light bullets is shown. This 3D isosurface is obtained by a direct numerical simulation of Eq. (3) with parameters $E_i = 1.21$, $\delta = 1.7$.

When dispersion and diffraction have the same influence, the formulation of this problem leads to the generalized Lugiato–Lefever equation (LLE) [18], describing the dynamics of nonlinear optical cavities as the one shown in Fig. 1. In its 3D form, the LLE reads [10,18]

$$t_r \frac{\partial E}{\partial t} = \sqrt{\theta} E_i - (\kappa + i\phi - i\gamma l |E|^2) E + i\left(\frac{l}{2q}\nabla_\perp^2 + \frac{\beta_2 l}{2}\frac{\partial^2}{\partial \tau^2}\right) E, \quad (1)$$

where $E = E(x, y, \tau, t)$ is the normalized slowly varying envelope of the intracavity field, and E_i is the input field amplitude. The time t corresponds to the slow-time evolution of E over successive round-trips, whereas τ accounts for the fast time in a reference frame traveling at the group velocity of light in the Kerr medium. The cavity round-trip time is denoted by t_r and the total losses by κ. The 2D diffraction is described by the Laplace operator $\nabla_\perp^2 = \partial_{xx} + \partial_{yy}$ acting on the transverse plane (x, y). The diffraction coefficient is inversely proportional to the wave number in the cavity material $q = \omega_0 n/c = 2\pi n/\lambda_0$, where ω_0 is the injected field frequency, λ_0 is the wavelength in vacuum, n is the linear refractive index, and c is the speed of light. The second derivative with respect to τ describes the group velocity dispersion. The chromatic dispersion coefficient β_2 is considered to be positive assuming that the Kerr cavity operates in the anomalous dispersion regime. The nonlinearity coefficient is $\gamma = n_2\omega_0/(cA_{\text{eff}})$, with n_2 being the nonlinear refractive index of the Kerr material considered. The effective area A_{eff} is the surface illuminated in the transverse plane. The transmission coefficient θ is the same for the input and the output mirrors $M_{1,2}$, and θ is supposed to be much smaller than unity. The length of the cavity is denoted by l and $\phi = 2\pi l/\lambda_0$ is the linear phase shift accumulated by the intracavity field over the cavity length l. To simplify further and to reduce the number of parameters describing the time evolution of the intracavity field, we introduce the following changes:

$$(x, y) \to \sqrt{\frac{l}{2q\kappa}}(x, y), \quad (t, \tau) \to \left(\frac{t_r}{\kappa}t, \sqrt{\frac{\beta_2 l}{2\kappa}}\tau\right),$$
$$E_i \to \kappa\sqrt{\frac{\kappa}{\gamma\theta l}}E_i, \quad \text{and} \quad E \to \sqrt{\frac{\kappa}{\gamma l}}E. \quad (2)$$

Under these changes, the generalized LLE (1) takes its dimensionless form

$$\frac{\partial E}{\partial t} = E_i - (1 + i\delta)E + i\left(\nabla_\perp^2 + \frac{\partial^2}{\partial \tau^2}\right)E + i|E|^2 E, \quad (3)$$

where $\delta = \phi/\kappa$ is the cavity detuning parameter. The homogeneous stationary solutions of LLE E_s are given by $E_i^2 = |E_s|^2[1 + (\delta - |E_s|^2)^2]$. For $\delta < \sqrt{3}$, the transmitted intensity as a function of the input intensity E_i^2 is single valued, whereas bistability occurs for $\delta > \sqrt{3}$. The steady-state homogeneous solution undergoes a modulational instability at the threshold value, $E_{\text{ic}}^2 = 1 + (\delta - 1)^2$ for the injected field intensity. The corresponding intracavity intensity is $|E_c|^2 = 1$ [18]. At this bifurcation point, the wavelength of 3D patterns is $\Lambda = 2\pi/\sqrt{2 - \delta}$.

A weakly nonlinear theory has been performed in 3D settings [10]. This analysis has revealed the predominance of the body-centered-cubic (bcc) lattice structure over a variety of 3D structures in the cavity field intensity [10]. The validity of this analysis is restricted to the values of the detuning parameter within the range $\delta < 41/30$. In what follows, we focus on the strongly nonlinear regime where modulational instability is subcritical, i.e., $\delta > 41/30$. Remarkably, besides the emergence of bcc structures, the same mechanism predicts the possible existence of stable dissipative LBs. An example of a single light bullet is shown in Fig. 2(a). This structure is obtained by a numerical simulation of Eq. (3) by using periodic boundary conditions in all directions. The initial condition used consists of a Gaussian function added to the value of the homogeneous steady state with an amplitude comparable to one of the periodic bcc structures. The cross section of the single LB along the transverse plane is shown in Fig. 2(i). The spatial profile of this 3D solution indicates that LBs possess a damped oscillatory tail. This single LB is obtained by a direct numerical simulation of Eq. (3), which can also be solved by assuming a spherical approximation. In this case, the stationary LB has the form $E(r) = E_s[1 + A(r)]$ with $r = (x^2 + y^2 + \tau^2)^{1/2}$ and with boundary conditions $A(0) = A_0(\neq 0)$, $\partial_r A(0) = 0$, and $A(r \to \infty) = 0$. The two profiles, one obtained from a direct numerical simulation and the other using the

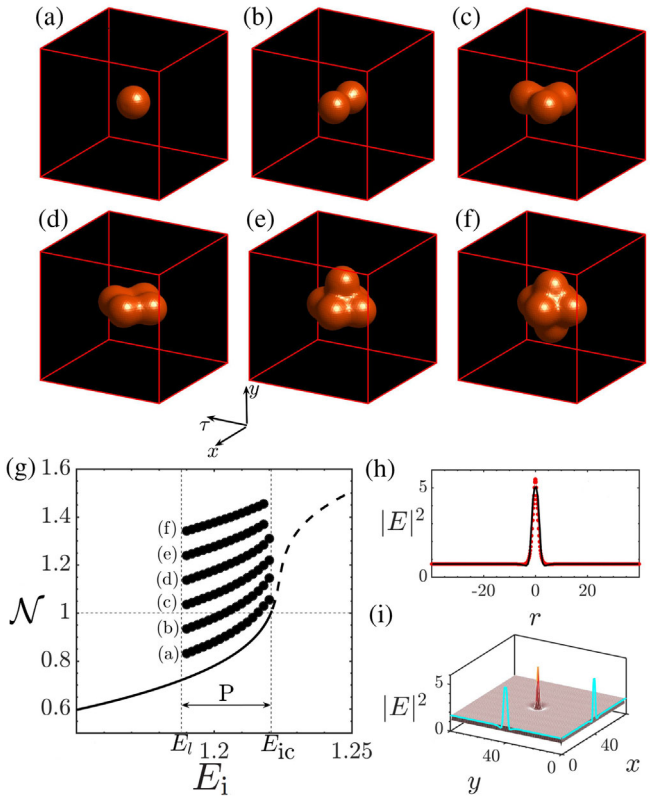

FIG. 2. Clusters of closely packed light bullets involving 1–6 LBs are shown respectively by the 3D isosurface in (a)–(f). (g) 3D bifurcation diagram associated with the LBs. The continuous black line denotes the stationary steady state. The pinning range is indicated by P. (h) Comparison between the LB obtained by a spherical symmetry (red dotted line) and the cross section along 1D direction of the single LB denoted by (a) represented by a continuous black line. (i) Cross section along the transverse plane of the single LB denoted by (a) with the profiles exhibiting decaying spatial oscillations. Parameter settings are $E_i = 1.21, \delta = 1.7$.

spherical symmetry approximation, are in good agreement, as shown in Fig. 2(h). The width of the LB is close to $\approx \pi/\sqrt{2-\delta}$, which is half the critical wavelength at the modulational instability.

Numerically, the challenge posed by the 3D LLE arises from the strongly nonlinear term, which when discretized leads to a large system of coupled strongly nonlinear stiff ordinary differential equations [19]. Because of this reason, the 3D simulations of LLE are still missing in the literature. It is to be noted that finite-difference methods can sometimes lead to spurious solutions that are nonphysical [19], which is where higher-order spectral methods come to the fore. In the present Letter, the spatial discretization of the LLE is done using a Fourier spectral method with periodic boundary conditions [19,20], and the time stepping is carried out with a fourth-order exponential time differencing Runge–Kutta scheme [20]. The main advantage of using a Fourier spectral method lies in the fact that the linear term of the discretized set of equations is diagonal, and more importantly, the nonlinear term is evaluated in physical space and then transformed to Fourier space. Further details on these methods can be found in these excellent books [19,20]. All the numerical simulations in the present Letter are carried out on a periodic domain of size 80 units in each direction, resolved using 128 grid points, with a time step of 0.01.

When initial conditions are set to two Gaussian shells centered at different positions in $E(x, y, \tau)$ space, these two perturbations evolve toward the formation of two bounded LBs, as can be seen on Fig. 2(b). By placing different LBs close to each other in the cavity, clusters of stable bounded states of LBs can be formed. When the individual LBs are well separated from one another, they are independent. However, when they are brought closer to each other, they start to interact via their oscillatory, exponentially decaying tails. The number of LBs and their distribution in the (x, y, τ) space is large. Some examples of closely packed LBs are shown in Figs. 2(c)–2(f). More precisely, Eq. (3) admits an infinite set of 3D solutions if the size of the system is infinite, with the limiting case corresponding to the infinitely extended periodic pattern distribution. These solutions are obtained for the same values of parameters, and they differ only by the seeded initial conditions. All these LBs coexist as stable solutions with the bcc lattice in the range P shown in Fig. 2, often called the pinning range [21]. These LBs are confined in (x, y, τ), and can be seen as a cluster of the elemental structure (a single LB) with a well-defined size, which are robust and stable.

The bifurcation diagram of these closely packed clusters of LBs is shown in Fig. 2(g) where the difference in intensity of the LB with respect to the background state, $\mathcal{N} = \int |E - E_s|^2 dxdyd\tau$ is shown as a function of the injected field E_i for a fixed value of the detuning parameter δ. The associated label is denoted next to the bifurcation curves. In the pinning range P, the system exhibits a high degree of multistability. The multiplicity of these 3D solutions of the LLE is strongly reminiscent of homoclinic snaking, indicating that the formation of bounded LB states and clusters of them is indeed a very robust phenomenon. Homoclinic snaking type of bifurcation has been investigated in one-dimensional settings [22]. It was first studied in relation with the Swift-Hohenberg equation [23] and is also a well-documented issue in spatially extended systems (see overviews [24]). This phenomenon, however, has never been documented in 3D settings. Note, however, that the 3D LBs in the LLE with a simple driving term does not admit vortex solutions, while other 3D vortices with embedded vorticity have been reported in [25]. We now provide a possible set of experimental parameter values. The link between the physical and the nondimensional parameters and variables are given by Eq. (2). The experimental setup consists of a broad area Fabry–Perot cavity filled with a material

having high Kerr coefficient and driven by a coherently injected beam. We suggest using chalcogenide glass, which is characterized by a very strong Kerr effect. To be more concrete, let us consider some typical physical parameters values. The nonlinear refractive index n_2 coefficient is as high as $n_2 \approx 2.3 \times 10^{-17}$ m^2/W. This results in a nonlinearity coefficient of $\gamma \approx 0.144$ W^{-1} km^{-1} for an effective (illuminated) area of $A_{\text{eff}} = 25 \times 10^4$ μm^2. The length of the cavity is $l = 1000$ μm and the reflectivity of the mirrors $1 - \theta = 0.95$, so that the optical losses are determined by the mirror transmission as the intrinsic material absorption loss can be as small as 40 dB/km. The wavelength $\lambda_0 = 4$ μm is chosen close to the zero dispersion wavelength. With these realistic physical parameters, the intensity of the injected field should be on the order of 10 MW/cm^2. This is reasonable since it is well below the damage threshold of chalcogenides, which can be as high as 1 GW/cm^2. The choice of these physical parameters are from [26]. In these settings, we expect that the spatial width in (x, y) plane will be $\approx$270 μm and the temporal width of the LB will be $\approx$0.08 ps for a value of $\beta_2 \approx 20$ ps^2/km.

When increasing the injected field intensity E_i beyond the pinning range P, LBs are observed to undergo transition via period doubling to a complex spatiotemporal regime. In the remainder of this Letter, we will characterize this complex regime. At high values of E_i, the occurrence of rogue waves in one- [27] and two-dimensional optical Kerr cavities has been recently shown [28]. The research on extreme events or rogue waves has gathered significant interest, especially in the fields of hydrodynamics and nonlinear optics, as witnessed by recent review papers [29,30]. Rogue waves are rare pulses with amplitudes significantly larger than the average one that arise due to self-focusing of energy of a wave group into one majestic event. We investigate this phenomenon in 3D settings, and we assume that the cavity operates in the monostable regime.

Figure 3(a) shows a 3D isosurface of the intensity in the cavity. Figure 3(b) shows a two-dimensional cut along the transverse plane, demonstrating an event with optical intensity significantly larger than the average amplitude of the background state. The three-dimensional perspective [Fig. 3(a)] shows the complex spatiotemporal regime at this high value of E_i. To quantify such extreme events, starting from a random initial condition, a statistical analysis based on the pulse amplitudes observed within the optical cavity is registered. Figure 3(c) shows the probability distribution of the number of events as a function of the intensity of the pulses in semilogarithmic scale for two different values of E_i. When E_i is increased beyond E_{ic}, though the system enters into a complex dynamical regime, the tail of the pulse height distribution stays below the threshold of twice the significant wave height. This can be seen in Fig. 3(c),

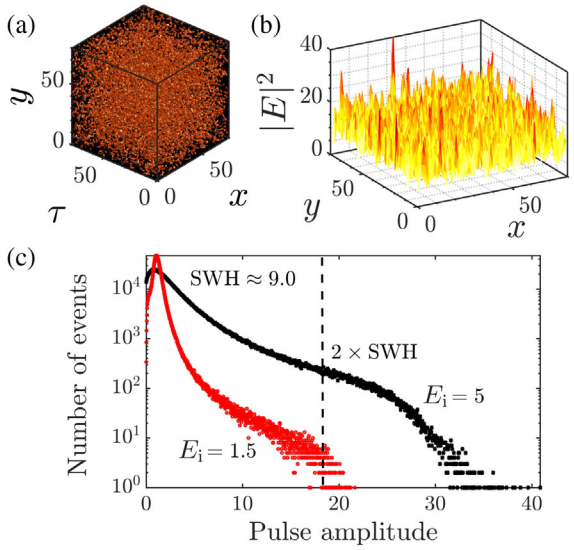

FIG. 3. Three-dimensional rogue waves. (a) A 3D isosurface of rogue waves in the cavity obtained for $E_i = 5$. (b) The cross section along the transverse (x, y) plane reveals an extreme event. (c) The probability distribution of the number of events as a function of the intensity of the pulses in semilogarithmic scale for two different values of E_i. The dashed line indicates events of amplitudes twice the SWH for $E_i = 5$. Parameter settings are $\delta = 1.7$.

where the statistical analysis at $E_i = 1.5$ is shown in red. As E_i is further increased, there is a considerable number of events with the maxima of intracavity intensity more than 2x the SWH, with even events of pulse amplitude as high as 4x the SWH. This can be seen from the statistical analysis shown in Fig. 3(c) for $E_i = 5$. In this complex spatiotemporal regime, the non-Gaussian statistical distribution of the wave intensity can be clearly seen with a long tail probability distribution. As remarked earlier, this is the main signature typical of rogue wave formation. These large intensity pulses belong to the class of rogue waves or extreme events [28,29]. We would like to emphasize that rogue waves are only formed in the LLE model when the spatiotemporal complexity is well developed, i.e., when the neighboring pulses in the oscillating pattern are interacting strongly. Even when the peak amplitude of the pulses clearly display complex dynamics, as in the case of $E_i = 1.5$ [Fig. 3(c)], no rogue waves are formed in the system. This is reflected in the tail of the pulse height distribution, which stays below the threshold of 2x SWH.

In conclusion, we have explicitly demonstrated the existence of robust three-dimensional dissipative solitons in the form of light bullets, leading to a striking light power confinement. The LBs result from the combined action of dispersion and diffraction mediated by Kerr nonlinearity, dissipation, and pumping. They could exist as isolated light bullets or in clusters of bounded states. They are dissipative three-dimensional structures that travel with the group velocity of light within the Kerr cavity. We have established

the link of this phenomenon with the homoclinic snaking type of bifurcation. When increasing further the intensity of the injected field, we have observed the transition from a stationary distribution of LBs to a complex regime. The statistical analysis has revealed evidences of 3D rogue waves with abnormal amplitudes larger than twice the significant wave height. Finally, we have provided realistic parameters for an experimental observation in an optical resonator filled with chalcogenide glass. These individually addressable LBs can bring a significant benefit for 3D optical storage, paving the way for future experimental research.

This work was supported in part by the Fonds Wetenschappelijk Onderzoek-Vlaanderen FWO (G0E5819N). We also acknowledge the support from the French National Research Agency (LABEX CEMPI, Grant No. ANR-11- LABX-0007), as well as the French Ministry of Higher Education and Research, Hauts de France Council, and European Regional Development Fund (ERDF) through the Contrat de Projets Etat-Region (CPER Photonics for Society P4S). M. T. acknowledges financial support from the Fonds de la Recherche Scientific FNRS under Grant CDR No. 35333527 "Semiconductor optical comb generator." A part of this work was supported by the "Laboratoire Associé International" University of Lille—ULB on "Self-organisation of light and extreme events" (LAI-ALLURE)."

*Corresponding author.
shyam7sunder@gmail.com

[1] P. Glansdorff and I. Prigogine, *Thermodynamic Theory of Structure, Stability and Fluctuations* (Wiley-Interscience, 1971); M. C. Cross and P. C. Hohenberg, Rev. Mod. Phys. **65**, 851 (1993); N. Rosanov, *Spatial Hysteresis and Optical Patterns* (Elsevier, New York, 1996), pp. 1–60; J. D. Murray, *Mathematical Biology: I. An Introduction* (Springer, Berlin, 2002); *Dissipative Solitons: From Optics to Biology and Medicine*, edited by N. Akhmediev and A. Ankiewicz, Lecture Notes in Physics Vol. 751 (Springer, Heidelberg, Germany, 2008).

[2] N. Akhmediev and A. Ankiewicz, *Solitons: Nonlinear Pulses and Beams* (Chapman & Hall, London, 1997); Y. K. Chembo, D. Gomila, M. Tlidi, and C. R. Menyuk, Eur. Phys. J. D **71**, 299 (2017); B. A. Malomed and D. Mihalache, Rom. J. Phys. **64**, 106 (2019); L. Lugiato *et al.*, *Nonlinear Optical Systems* (Cambridge University Press, Cambridge, England, 2015).

[3] A. J. Scroggie, W. J. Firth, G. S. McDonald, M. Tlidi, R. Lefever, and L. A. Lugiato, Chaos Solitons Fract. **4**, 1323 (1994).

[4] F. Leo, S. Coen, P. Kockaert, S.-P. Gorza, P. Emplit, and M. Haelterman, Nat. Photonics **4**, 471 (2010).

[5] V. Odent, M. Taki, and E. Louvergneaux, New J. Phys. **13**, 113026 (2011).

[6] S. Coen, H. G. Randle, T. Sylvestre, and M. Erkintalo, Opt. Lett. **38**, 37 (2013); L. Lugiato, F. Prati, M. L. Gorodetsky, and T. J. Kippenberg, Phil. Trans. R. Soc. A **376**, 20180113 (2018).

[7] F. Ferdous, H. Miao, D. E. Leaird, K. Srinivasan, J. Wang, L. Chen, L. T. Varghese, and A. M. Weiner, Nat. Photonics **5**, 770 (2011); T. J. Kippenberg, R. Holzwarth, and S. A. Diddams, Science **332**, 555 (2011).

[8] V. B. Taranenko, I. Ganne, R. J. Kuszelewicz, and C. O. Weiss, Phys. Rev. A **61**, 063818 (2000); S. Barland *et al.*, Nature (London) **419**, 699 (2002); D. Mihalache, Rom. J. Phys. **59**, 295 (2014); M. Tlidi, M. Taki, and T. Kolokolnikov, Chaos **17**, 037101 (2007); M. Tlidi, K. Staliunas, K. Panajotov, A. G. Vladimirov, and M. G. Clerc, Phil. Trans. R. Soc. A **372**, 20140101 (2014).

[9] Y. Silberberg, Opt. Lett. **15**, 1282 (1990); D. E. Edmundson, Phys. Rev. E **55**, 7636 (1997).

[10] K. Staliunas, Phys. Rev. Lett. **81**, 81 (1998); M. Tlidi, M. Haelterman, and P. Mandel, Quantum Semiclass. Opt. **10**, 869 (1998).

[11] M. Brambilla, T. Maggipinto, G. Patera, and L. Columbo, Phys. Rev. Lett. **93**, 203901 (2004); L. Columbo, I. M. Perrini, T. Maggipinto, and M. Brambilla, New J. Phys. **8**, 312 (2006).

[12] N. A. Kaliteevskiĭ and N. N. Rosanov, Opt. Spectrosc. **89**, 569 (2000); N. Veretenov, A. G. Vladimirov, N. A. Kaliteevskii, N. N. Rozanov, S. V. Fedorov, and A. N. Shatsev, Opt. Spectrosc. **89**, 380 (2000); M. Marconi, J. Javaloyes, S. Balle, and M. Giudici, Phys. Rev. Lett. **112**, 223901 (2014); J. Javaloyes, Phys. Rev. Lett. **116**, 043901 (2016); F. Dohmen, J. Javaloyes, and S. V. Gurevich, Chaos **30**, 063120 (2020); N. Veretenov and M. Tlidi, Phys. Rev. A **80**, 023822 (2009); N.-C. Panoiu, R. M. Osgood, B. A. Malomed, F. Lederer, D. Mazilu, and D. Mihalache, Phys. Rev. E **71**, 036615 (2005).

[13] C. Milián, Y. V. Kartashov, and L. Torner, Phys. Rev. Lett. **123**, 133902 (2019).

[14] B. A. Malomed, D. Mihalache, F. Wise, and L. Torner, J. Opt. B **7**, R53 (2005).

[15] M. Tlidi and P. Mandel, Phys. Rev. Lett. **83**, 4995 (1999); I. Bordeu and M. G. Clerc, Phys. Rev. E **92**, 042915 (2015).

[16] C. Kharif *et al.*, *Rogue Waves in the Ocean* (Springer Science & Business Media, New York, 2008).

[17] D. R. Solli, C. Ropers, P. Koonath, and B. Jalali, Nature (London) **450**, 1054 (2007).

[18] L. A. Lugiato and R. Lefever, Phys. Rev. Lett. **58**, 2209 (1987); M. Tlidi, M. Haelterman, and P. Mandel, Europhys. Lett. **42**, 505 (1998).

[19] W. B. Jones and J. O'Brian, Chaos **6**, 219 (1996); A. Kassam, *High Order Timestepping for Stiff Semilinear Partial Differential Equations* (University of Oxford, Oxford, 2004).

[20] L. N. Trefethen, *Spectral Methods in MATLAB* (SIAM, Philadelphia, 2000); Y. Saad, *Numerical Methods for Large Eigenvalue Problems* (SIAM, Philadelphia, 2011); S. M. Cox and P. C. Matthews, J. Comput. Phys. **176**, 430 (2002).

[21] Y. Pomeau, Physica (Amsterdam) **23D**, 3 (1986).

[22] D. Gomila, A. J. Scroggie, and W. J. Firth, Physica (Amsterdam) **227D**, 70 (2007); M. Tlidi and L. Gelens, Opt. Lett. **35**, 306 (2010); P. Parra-Rivas, D. Gomila, M. A.

Matias, S. Coen, and L. Gelens, Phys. Rev. A **89**, 043813 (2014).
[23] P. D. Woods and A. R. Champneys, Physica (Amsterdam) **129D**, 147 (1999); P. Coullet, C. Riera, and C. Tresser, Phys. Rev. Lett. **84**, 3069 (2000).
[24] J. Burke and E. Knobloch, Chaos **17**, 037102 (2007); E. Knobloch, Annu. Rev. Condens. Matter Phys. **6**, 325 (2015).
[25] D. Mihalache, D. Mazilu, F. Lederer, Y. V. Kartashov, L. C. Crasovan, L. Torner, and B. A. Malomed, Phys. Rev. Lett. **97**, 073904 (2006); V. Skarka, N. B. Aleksic, H. Leblond, B. A. Malomed, and D. Mihalache, Phys. Rev. Lett. **105**, 213901 (2010); N. A. Veretenov, S. V. Fedorov, and N. N. Rosanov, Phys. Rev. Lett. **119**, 263901 (2017); N. N. Rosanov, S. V. Fedorov, and N. A. Veretenov, Eur. Phys. J. D **73**, 141 (2019).
[26] G. Snopatin, V. S. Shiryaev, V. G. Plotnichenko, E. M. Dianov, and M. F. Churbanov, Inorg. Mater. (USSR) **45**, 1439 (2009); A. Zakery, *Optical Nonlinearities in Chalcogenide Glasses and Their Applications* (Springer, New York, 2007).
[27] A. Coillet, J. Dudley, G. Genty, L. Larger, and Y. K. Chembo, Phys. Rev. A **89**, 013835 (2014).
[28] M. Tlidi and K. Panajotov, Chaos **27**, 013119 (2017); K. Panajotov, M. G. Clerc, and M. Tlidi, Eur. Phys. J. D **71**, 176 (2017).
[29] N. Akhmediev, J. M. Dudley, D. R. Solli, and S. K. Turitsyn, J. Opt. **15**, 060201 (2013); M. Onorato, S. Residori, U. Bortolozzo, A. Montina, and F. T. Arecchi, Phys. Rep. **528**, 47 (2013); B. Kibler, A. Chabchoub, A. Gelash, N. Akhmediev, and V. E. Zakharov, Phys. Rev. X **5**, 041026 (2015); N. Akhmediev *et al.*, J. Opt. **18**, 063001 (2016).
[30] M. L. McAllister, S. Draycott, T. A. A. Adcock, P. H. Taylor, and T. S. van den Bremer, J. Fluid Mech. **860**, 767 (2019); J. M. Dudley, G. Genty, A. Mussot, A. Chabchoub, and F. Dias, Nat. Rev. Phys. **1**, 675 (2019); K. Panajotov, M. Tlidi, Y. Song, and H. Zhang, Chaos **30**, 053103 (2020).